Thermal behaviour of zircon/zirconia-added chemically durable borosilicate porous glass

M. Hasanuzzaman[1*], M. Sajjia[1], A. Rafferty[2], A. G. Olabi[1]

[1]*Dublin City University, Mechanical and Manufacturing Engineering, Dublin 9, Ireland*
[2]*Trinity College Dublin, Centre for Research on Adaptive Nanostructures and Nanodevices, Dublin 2, Ireland*
**Corresponding author. Tel.: +353-1-7007718, Fax: +353-1-7007148*
E-mail address: hasanum2@mail.dcu.ie

Abstract
Macroporous alkali resistant glass has been developed by making additions of zirconia (ZrO_2) and zircon ($ZrSiO_4$) to the sodium borosilicate glass system SiO_2-B_2O_3-Na_2O. The glass was made using a traditional high temperature fusion process. Differential thermal analysis (DTA) was carried out to identify the glass transition temperature (T_g) and crystallisation temperature (T_x). Based on these findings, controlled heat-treatments were implemented to separate the glass into two-phases; a silica-rich phase, and an alkali-rich borate phase. X-ray diffraction (XRD) was used to identify any crystal phases present in the as-quenched and heat-treated glasses. Fourier transform infrared (FTIR) spectroscopy also proved effective in investigating phase separation and crystallisation behaviour. After leaching, a silica-rich skeleton with an interconnected pore structure and a uniform pore distribution was observed. Pore characterisation was carried out using mercury porosimetry. The size and shape of the pores largely depended on the heat-treatment temperature and time. ZrO_2/$ZrSiO_4$ additions increased the alkali resistance of the porous glass 3-4 times.

Keywords: Porous glasses; Borosilicate glass; Phase separation; Glass transition; Alkali resistance.

1. Introduction

Borosilicate glass has been of interest for more than two decades due to its diversified use in the biological, electrical and pharmaceutical industries. It is known for its superior usability in membrane technology, size exclusion and affinity protein chromatography (separation science) [1-3]. For more than thirty years, borosilicate glass has been used for the entrapment/immobilisation of high level waste from nuclear power plants and arms industries [4-6]. A low dielectric constant and negligible thermal expansion coefficient make it suitable for microelectronic packaging [7,8]. Moreover, the usage of borosilicate glass as a reinforced matrix component in composites to improve mechanical properties is widely accepted [9]. Increasing the chemical durability is one of the major challenges for porous borosilicate glass, to make it suitable and re-usable for many other applications [10]. Borosilicate glass is known for its phase separation characteristics, thus enabling Controlled Pore Glass (CPG) of micro-meso- and macro-pore size, depending on the heating cycle [11].

Porous glass can be derived from a glass which is heat-treated (HT) to form two interconnecting phases. The heat-treated glass is then leached selectively to remove one of the phases. The heat-treatment step and leaching conditions can be tailored to achieve the desired pore size, pore volume and surface area. Common production methods include traditional glass melting or sol-gel. The glass composition plays a major role in the phase separation behaviour of glasses under certain heat treatment conditions.

Figure 1 shows the critical temperature zones in the ternary SiO_2-B_2O_3-Na_2O system, where phase separation occurs. Figure 1 also shows the tie-lines, demarcating the compositions and concentrations of phases present in different temperature zones.

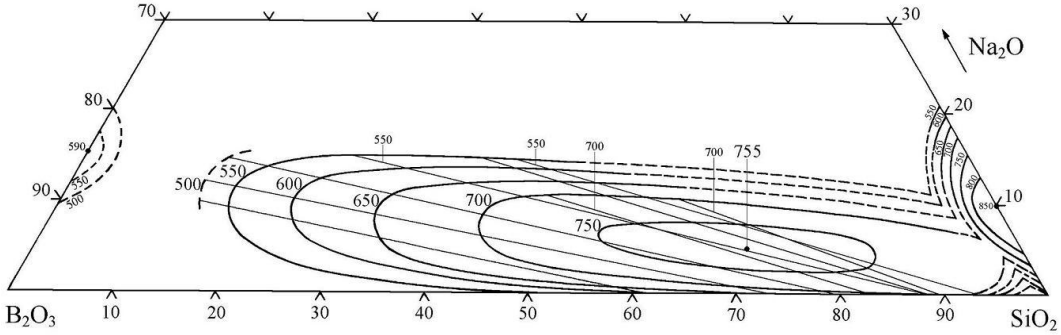

Figure 1: Phase separation in the sodium borosilicate glass system [12]. Dashed lines are uncertain.

Zirconia containing porous glasses have received attention as a means of increasing the alkali resistance of borosilicate glass [13-15]. In this study, the thermal behaviour of sodium borosilicate glasses with additions of zirconia and zircon were investigated. Based on the thermal behaviour characteristics of different compositions, heat-treatment times and temperatures were optimized to achieve well-defined porous morphologies.

2. Experimental

2.1 Glass preparation

The compositions of glasses prepared in this study are shown in Table 1. ZrO_2 was added to the SiO_2-B_2O_3-Na_2O system with the amount of alkali oxide (Na_2O) varied between 6 wt% and 10 wt%. For addition of $ZrSiO_4$, the amount of alkali oxide (Na_2O) is fixed at 6 wt%. Compositions B-E involve substitution of SiO_2 with gradually increasing amounts of ZrO_2, keeping the content of Na_2O at 10 wt%, whilst composition E-II contained 6 wt% of Na_2O. Composition EE was the same as E-II, but with $ZrSiO_4$ replacing ZrO_2. SiO_2, B_2O_3, Na_2CO_3, ZrO_2 and $ZrSiO_4$ powders were procured from Sigma-Aldrich (Ireland). The glass reagents were ball-milled for 14 hours. The mixed batches were melted in zirconia crucibles (Almath Ltd., UK) at 1450°C for 2 h in an electric furnace. The melts were then water-quenched to produce frit. The glass frits were crushed in a ball mill for 12 h. The resultant powder was sieved to a particle size > 45 µm < 212 µm.

Table 1: Composition of glasses in wt%.

	Composition wt%				
Glass	SiO_2	B_2O_3	Na_2O	ZrO_2	$ZrSiO_4$
A	65	25	10	0	0
B	62	25	10	3	0
C	58	25	10	7	0
D	54	25	10	11	0
E	50	25	10	15	0
AA	69	25	6	0	0
E-II	54	25	6	15	0
EE	54	25	6	0	15

2.2 Thermal analysis

Differential Thermal Analysis (DTA) (Stanton Redcroft, UK) was used to measure the glass transition temperature (T_g) and to investigate the crystallisation behaviour. Heating rates of 10, 15, and 20 °C/min were employed using 30 mg of sample and alumina as a reference.

Dilatometry (Model 402 E, Netzsch Ltd., Germany) was used to determine the dilatometric softening temperature (T_d) and the glass transition temperature (T_g) of a bulk glass specimen which was a nominal cylinder of approximate dimensions 11.5 mm (L) x 3 mm (D). The specimen was heated in air at a rate of 10 °C/min from room temperature to 1000 °C.

2.3 Heat treatment

Thermal treatment to induce phase separation was carried out on glass powder (> 45 µm <212 µm particle size) using a horizontal tube furnace (Carbolite Ltd., Sheffield, UK) at a heating rate of 10 °C/min. The dwell temperature ranged from 630–700 °C and the dwell time was 14–63 h, depending on composition.

2.4 X-Ray Diffraction Analysis (XRD) and Fourier Transform Infrared (FTIR) Spectroscopy

Non heat-treated and heat-treated glass powders were analyzed using XRD. A Bruker advanced D8 X-ray diffractometer with Ni-filtered Cu Kα radiation of wavelength 1.5406 Å at 40 kV and 40 mA was used to measure the XRD patterns with a step size of 0.1° in a range of 2θ values from 10 to 80° at scanning speed of 10 sec/step. Crystalline phases present in heat-treated glass samples were identified by the positions listed in the Joint Commission on Powder Diffraction Standards (JCPDS) files. The FTIR spectra were obtained using a Perkin-Elmer GX instrument with a resolution of 16 cm^{-1} in the range 400 cm^{-1} to 4000 cm^{-1}.

2.5 Glass leaching

A heating bath, magnetic stirrer, and condenser were used to conduct glass leaching experiments. The heat-treated glasses were first immersed in 1N HNO_3 for 24 h at 95-98 ºC to remove the borate phase, then in 3N H_2SO_4 for 24 h at 95-98 ºC to dissolve colloidal zirconia, and finally the gelated SiO_2 was washed out with 0.5N NaOH for 5 h at 25 ºC. An H_2SO_4 leaching step was found to be unnecessary for ZrO_2/$ZrSiO_4$ free compositions. A magnetic stirrer was used to prevent the glass powder from settling on the bottom of the flask and to make leaching more effective. Following leaching, the resultant glass powders were washed with water several times and dried for 12h at 120 °C.

2.6 Porosimetery

The experiments were performed on leached glass using mercury porosimetry (Autoscan-33 Porosimeter, Quantachrome, UK). Mercury intrusion and extrusion over a range of pressures (0-33000 PSIA) was performed, to determine pore sizes, pore volumes, pore surface areas and pore distributions.

2.7 Scanning Electron Microscopy (SEM)

Pore morphologies and pore sizes of the leached glasses were observed using SEM (EVO LS15, Carl Zeiss NTS GmbH, Germany).

2.8 Alkali resistance testing

The alkali resistance of leached glass samples was measured by incubating a 1 ml volume of sample in 10 ml of an aqueous sodium hydroxide solution (0.5N) for 24 h. Following this, the leachant was neutralised with 1N HCl acid and then washed in deionised water and dried at 100 °C for 18 h. After drying, each sample was weighed to an accuracy of 0.1 mg. The weight loss was then calculated in milligrams per square decimetre (mg/dm^2) using the surface area data from porosimetry.

3. Results and discussion

3.1 Thermal behaviour and XRD analysis

Figure 2 presents the DTA analysis of the glass powder sample AA, which had been sieved to a particle size > 45 µm < 212 µm, for a heating rate of 10 °C/min. The mean particle size diameter, D [4, 3], as determined by light scattering particle size analysis (Malvern Mastersizer S, Malvern Ltd., UK), was found to be 197 µm. In Figure 2, a change in slope is observed at about 478 °C and continues until it reaches 520 °C. Three characteristic temperatures can be used to define this endothermic gradient attributed to the glass transformation range. T_f is denoted as the onset glass transformation temperature, T_{mid} is the midpoint, and T_m is the maximum of the endothermic inflection. Kerĉ and Sĉiĉ considered another point after T_m which they denoted as the extrapolated end temperature (T_e) [16]. T_f and T_{mid} are generally accepted as the glass transition temperature (T_g) for most applications [17]. A broad exothermic event is observed in the range 740–900 °C. Surface crystallisation is considered the dominant mechanism, since no sharp exothermic peak was observed, even for DTA analysis of finer particle sizes, i.e. < 45µm.

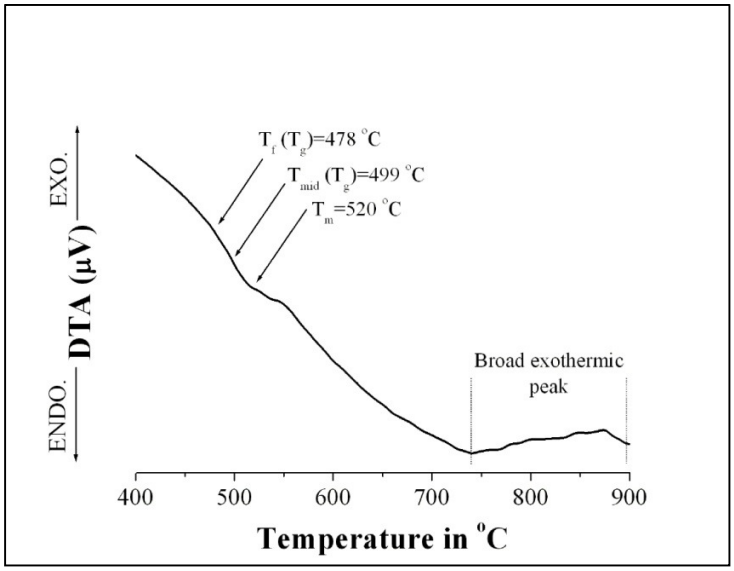

Figure 2: DTA curve of glass AA at a heating rate of 10 °C/min.

Figure 3 shows the linear thermal expansion curve of a bulk sample of glass AA heated at 10 °C/min. The glass expands until 305 °C, above which the glass contracts suddenly up to about 425 °C, before expanding again. This sudden expansion in the temperature range 430 °C to 520 °C is referred to as the transformation range and indicates the onset of viscoelastic behaviour, where bond breaking is predominant. The onset temperature of the transformation range at 430 °C is attributed to T_f. The DTA curve (see Figure 1) shows the glass transformation temperature of same sample (glass AA) at about 478 °C (T_f) with the same heating rate. The temperature of maximum expansion is identified at 550 °C and can be referred to as the dilatometric softening temperature (T_d). A sharp decrease in sample dimension is noticed at about 560 °C after the dilatometric softening temperature which corresponds to viscous flow of the sample under stresses imposed by the dilatometric push rod. Shelby [2] and Kingery [18] revealed a dramatic distinction in thermal expansion behaviour between quenched glasses and glasses which had been annealed prior to dilatometric characterisation. The quenched glasses showed very prominent

contraction-expansion characteristics. For annealed glasses the expansion-contraction was minimal and to a large extent 'washed out' as a result of annealing the glass above T_g. The expansion behaviour of glass AA (quenched) is in good agreement with the findings of Shelby and Kingery. From the dilatometric data, the linear thermal expansion coefficient (α_l) of glass AA was calculated as 4.77 x 10^{-6} °C^{-1} in the temperature range between room temperature and 300 °C, which is in good agreement with the measured expansion coefficient of similar sodium borosilicate glass compositions reported in the literature [19].

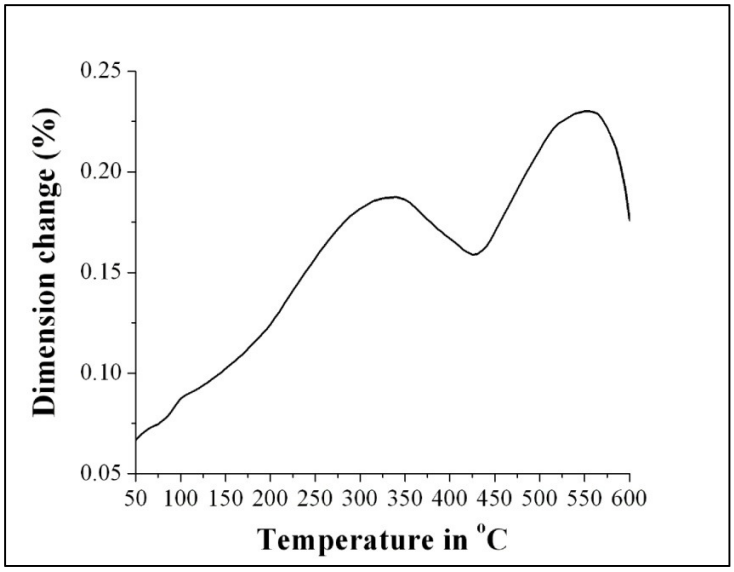

Figure 3: Linear thermal expansion curve of bulk glass AA obtained at 10 °C min^{-1}.

Figure 4 illustrates the linear shrinkage behaviour of a bulk sample of glass AA heated at 10 °C/min. The section of the curve within the dashed circle is shown in exaggerated detail in Figure 3. As can be seen in Figure 4, the bulk sample begins to shrink at about 560 °C and continues with a sharp fall upon reaching about 660 °C. Beyond 660 °C, there is no significant shrinkage observed. A total linear shrinkage of around 1.7% is observed. This shrinkage is attributed to viscous flow and continues until 660 °C.

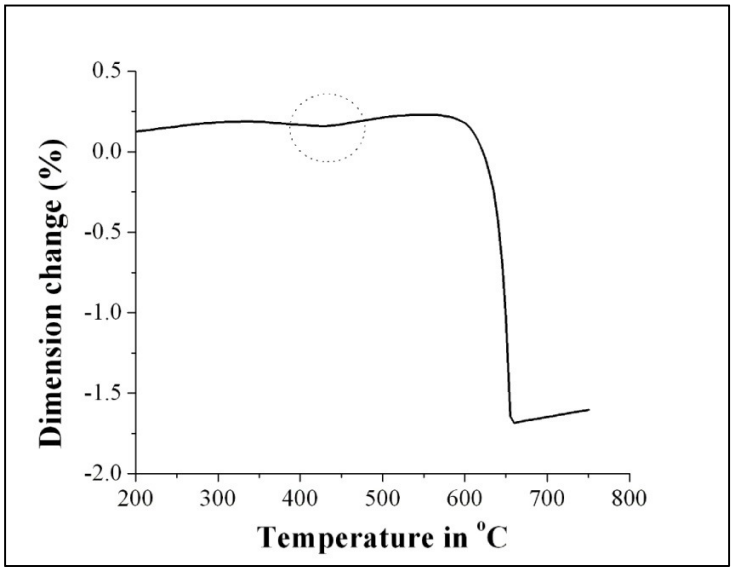

Figure 4: Linear shrinkage of bulk glass AA obtained at 10 °C min^{-1}.

Figure 5 presents XRD patterns for powder samples of glass AA which were heat-treated at 650 °C for different time periods (1 h, 3 h, 6 h and 14 h). The peaks at 2θ = 21.8°, 28.5°, 36 [JCPDS 01-0438, 03-0267] are assigned to cristobalite. Cristobalite peaks are observed in the powder sample heat-treated for 14 h. However, no crystallisation peaks appeared for a bulk sample of glass AA heat-treated under similar condition for 14 h. Other studies have shown that powder samples are more prone to surface crystallisation due to having far greater specific surface area than the bulk samples [17,20,21].

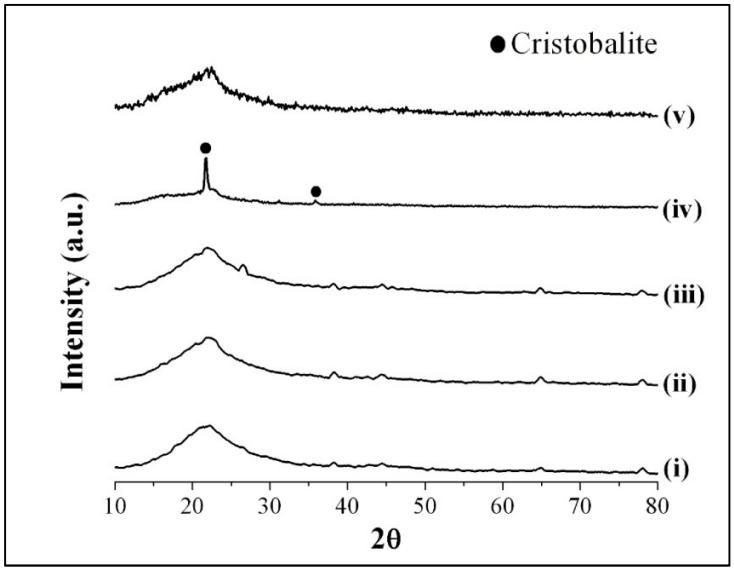

Figure 5: XRD patterns of glass AA heat treated at 650 °C for: (i) powder sample, 1 h; (ii) powder sample, 3 h; (iiii) powder sample, 6 h; (iv) powder sample, 14 h; (v) bulk sample, 14 h.

Figure 6 shows the DTA analysis of the glass powder sample EE for a heating rate of 15 °C/min. The mean particle size diameter, D [4, 3], was found to be 80.1 µm. In Figure 6, a change in slope is

observed at about 497 °C and continues until it plateaus at approximately 600 °C. The exothermic peak observed at 667 °C is attributed to crystallisation. The sharp nature of this peak, denoted as maximum crystallisation temperature (T_p), is indicative of bulk crystallisation [20-22]. This sharp peak was not observed for the glass AA which contained no $ZrSiO_4$, so clearly the zircon is promoting bulk crystallisation.

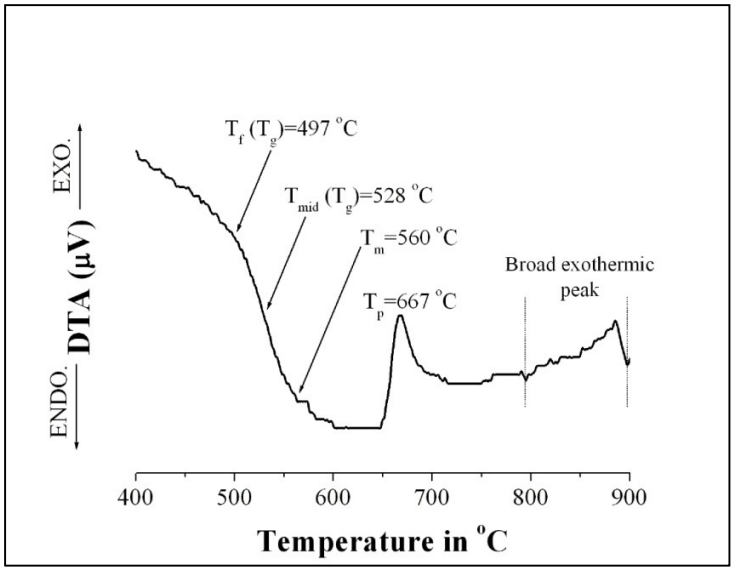

Figure 6: DTA curve of glass EE at a heating rate of 15 °C/min.

XRD analysis was performed on samples of glass composition EE to identify the crystallisation phases related to the exothermic peak observed in Figure 6. The samples were heat treated at 650 °C, i.e. T_p onset, for various durations (1 h, 14 h, 24 h and 63 h). Peaks assigned to tetragonal ZrO_2 ($2\theta = 30°$, 51°, 60) [JCPDS 02-0733] were identified for the sample heated at 650 °C for 1 h, 14 h, 24 h and 63 h (see Figure 7). The peaks at $2\theta = 21.8°$, 28.5°, 36 [JCPDS 01-0438, 03-0267] are attributed to cristobalite. For heat-treatments ≤ 24 h, the cristobalite peaks exhibit low intensities compared with the tetragonal ZrO_2 peaks. For heat-treatment durations of > 24 h < 63 h, the intensity of the peaks related to cristobalite increases. Crystallisation of cristobalite predominates over crystallisation of tetragonal ZrO_2 for heat-treatment times ≥ 24 h. Therefore, it can be considered that the T_p observed in Figure 6 is due to crystallisation of tetragonal zirconia.

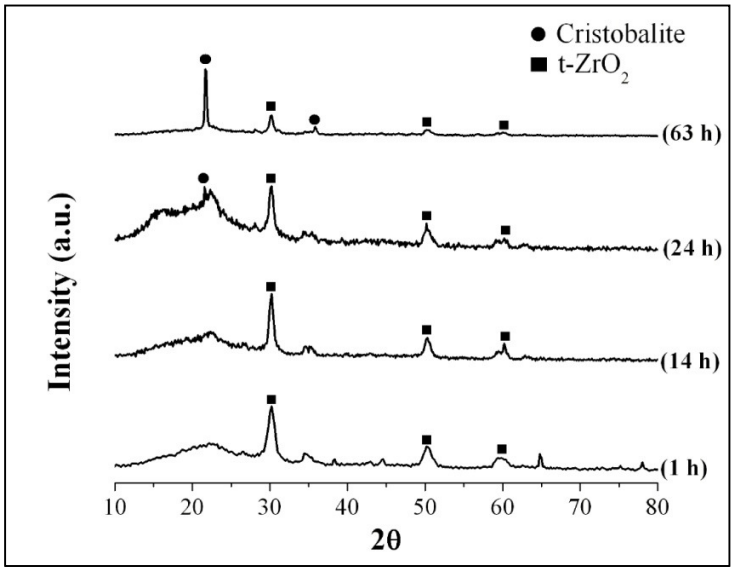

Figure 7: XRD patterns of glass EE heat treated at 650 °C for different times (1 h, 14 h, 24 h and 63 h).

Compared with composition EE, no well-defined exothermic peak was observed for composition E-II (see Figure 8). Onset of a broad exothermic event occurs at approximately 650 °C and is likely associated with surface crystallisation [20-23].

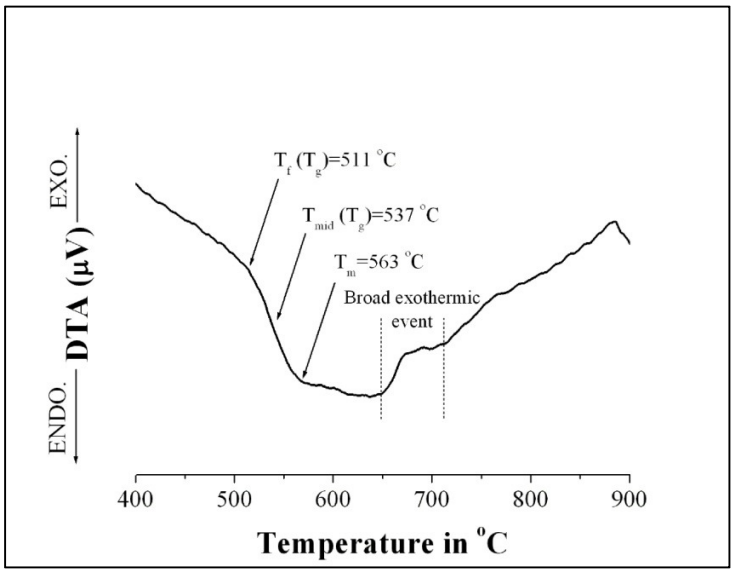

Figure 8: DTA curve of glass E-II at a heating rate of 10 °C/min.

Apart from the zircon-containing glass sample (EE), no sharp exothermic peaks were observed for the other glass compositions. Broad exotherms were observed, indicative of surface crystallisation. The results of DTA analysis for all samples are listed in Table 2. The T_f and T_m varied with the heating rate. Other authors found T_g heating rate dependency [2,24]. It is evident that T_f increases incrementally with increasing ZrO_2 content from 515 °C to 522 °C for the series A to E. Addition of ZrO_2 will increase the number of bridging oxygens per silicon atom and the presence of Zr^{4+} ions will impart a higher packing

density and higher T_g. This behaviour is consistent with the theory that ZrO_2 can act both as an intermediate and a network glass former [25]. It can also be noticed from Table 2 that glass A which contained more Na_2O (10 wt%) compared with AA (6 wt%) shows higher T_f. A similar trend is observed between glass E (10 wt% Na_2O, 15 wt% ZrO_2) and E-II (6 wt% Na_2O, 15 wt% ZrO_2). In sodium silicate glasses, increasing the alkali content breaks up the three-dimensional network with the formation of singly-bonded oxygens which do not participate in the network, thus reducing the length of the chain. The principal effect of increased alkali content is reduction in melting temperature by decreasing the viscosity and thus expecting lower T_g. However, an exception to this is observed for glasses containing B_2O_3, which is known as the boric oxide anomaly. Increasing alkali content in sodium borate glass compositions converts BO_3 triangles to BO_4 tetrahedra, thereby increasing the network connectivity. Therefore, the glass transition temperature increases. Non-bridging oxygen sites do not become apparent until the alkali content is increased up to about 30 mol% [26]. Glass E-II (15 wt% ZrO_2) and EE (15 wt% $ZrSiO_4$) show almost similar T_f values, indicating that the presence of zircon or zirconia in the glass has a similar impact on T_g.

Table 2: DTA results for three different heating rates (10°C/min, 15°C/min, 20°C/min)

	10 °C/min		15 °C/min		20 °C/min	
Glass	T_f	T_m	T_f	T_m	T_f	T_m
A	515	567	514	562	510	567
B	508	568	514	588	520	577
C	518	575	524	588	532	593
D	520	577	517	589	520	590
E	522	576	528	586	528	594
AA	478	520	472	522	468	522
E-II	511	563	503	577	504	597
EE	509	550	497	560	492	566

3.2 Using FTIR and XRD to detect crystallisation and phase separation

FTIR is widely used to interpret the structural modifications which occur during heat-treatment [27-29]. The FTIR spectrum of amorphous silica was reported in other studies and the major peak corresponding to the asymmetric Si–O–Si stretching vibration was recorded at approximately 1100 cm^{-1} [28,30]. The position of the Si–O–Si band changes depending on the type and amount of modifier cations introduced to the system [29,31]. Figure 9a shows the FTIR spectra of as-quenched and heat treated samples of Glass C. XRD analysis is also reported to correlate the findings (see Figure 9b). It can be noticed from the FTIR spectrum that the as-quenched, non-heat-treated glass has a peak shift of 49 cm^{-1} compared with amorphous silica. The Si–O–Si stretching peak is reported at 1051 cm^{-1}. The peak starts shifting towards a higher wave number as heat-treatment temperature increases to 680 °C. The peak shift then reverses towards a lower wavenumber for heat treatment temperature at 700 °C. The decrease in the IR peak wavenumber at 700 °C may be due to a decrease in the extent of phase separation. At lower temperature, e.g. at 630 °C, the immiscibility boundary is wide but at higher temperature it is near to the edges and thus the extent of phase separation could decrease. The increasing wavenumber with incremental heat-treatment temperature rise in the range 630–680 °C indicates a higher degree of phase separation and can be attributed to the increasing number of Si–O–Si bridging bonds [28,29]. The broad band at about 680 cm^{-1} can be assigned to BO_4 tetrahedrons [32]. A peak at 610–627 cm^{-1} appears in samples heat treated at comparatively high temperature (680°C and 700°C). The XRD study also

identifies the existence of cristobalite in these two samples. Therefore, the presence of the peak at 610–627 cm^{-1} can be correlated with the crystallisation process.

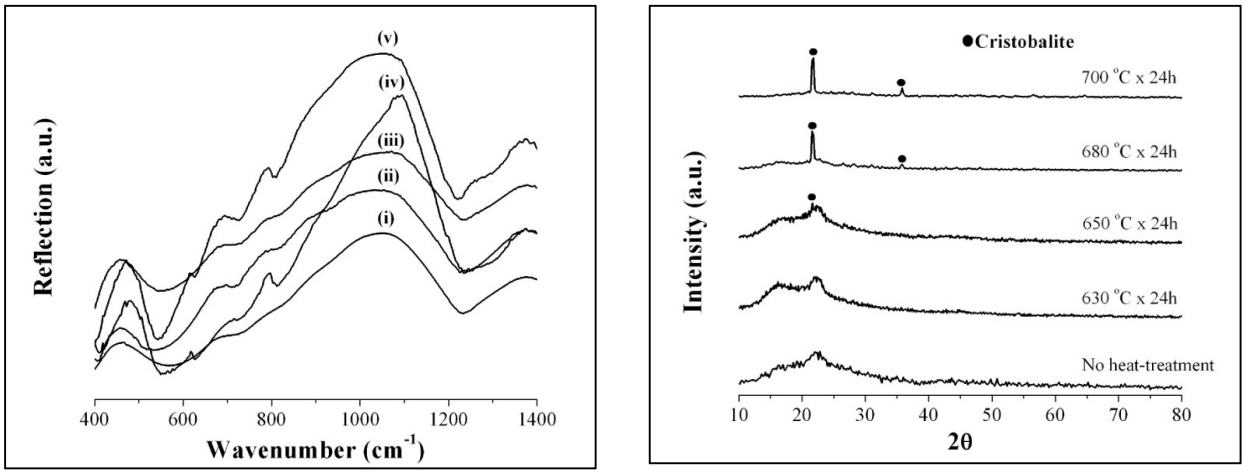

(a) (b)

Figure 9: (a) FTIR absorbance spectra of glass C as a function of heat-treatment: (i) before heat-treatment, (ii) 630 °C x 24 h, (iii) 650 °C x 24 h, (iv) 680 °C x 24 h, (v) 700 °C x 24 h; and (b) the XRD patterns showing crystal formation.

3.3 TTT diagram

Visual examination was carried out on samples phase separated using different heat-treatment times and temperatures. Figure 10 shows the Time Temperature Transformation (TTT) diagram for composition AA. The glass frit was visually clear initially and remained clear at certain temperature ranges, which suggests no phase separation. Faint opalescence increased as a function of both time and temperature. This is in accordance with another study where phase separation was defined by the visual appearance of glass exhibiting opalescence [15]. As can be seen from Figure 10, the minimum time required for crystallisation onset is at about 800 °C. With decreasing temperature, the time required for crystallisation onset increases. The TTT curve located below the crystallisation curve indicates the initiation of phase separation. At higher temperature (> 650 °C) and time (>350 min), the glass will experience phase separation coupled with crystallisation and the crystallisation increases with further extension of heat treatment time. It is also revealed from the TTT diagram that 630 °C would be an appropriate temperature for glass AA to initiate phase separation without crystallisation even for extended times.

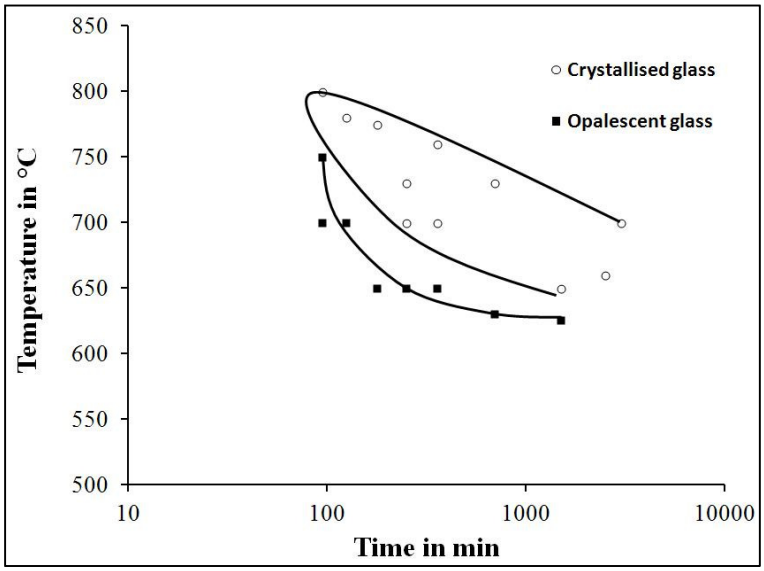

Figure 10: TTT diagram for Glass AA.

3.4 SEM observations

Skeleton-like microstructures with highly connected pores are observed for porous glasses of composition AA (Figure 11 b), E-II (Figure 11 c) and EE (Figure 11 d). These spherical droplet like pores with high degree of connectivity are usually formed by spinodal decomposition [15,33]. Whereas, spherical droplets with low connectivity observed with composition A (Figure 11 a) and composition C (Figure 12 b) which is believed due to nucleation and growth process [33].

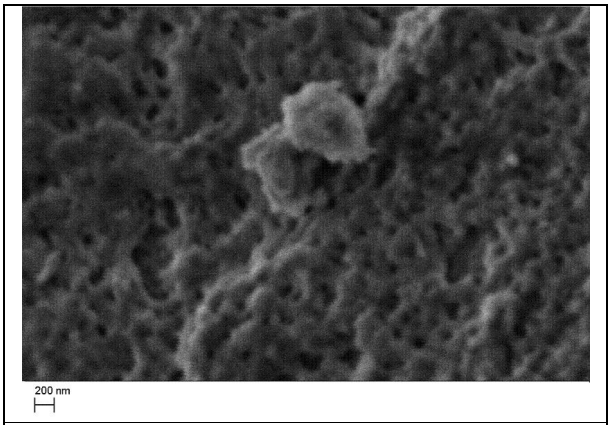

(a)

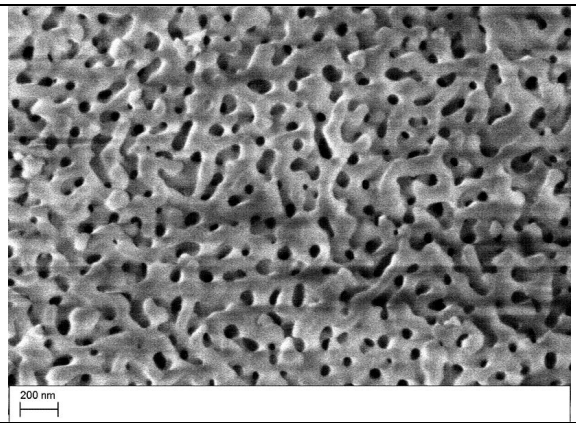

(b)

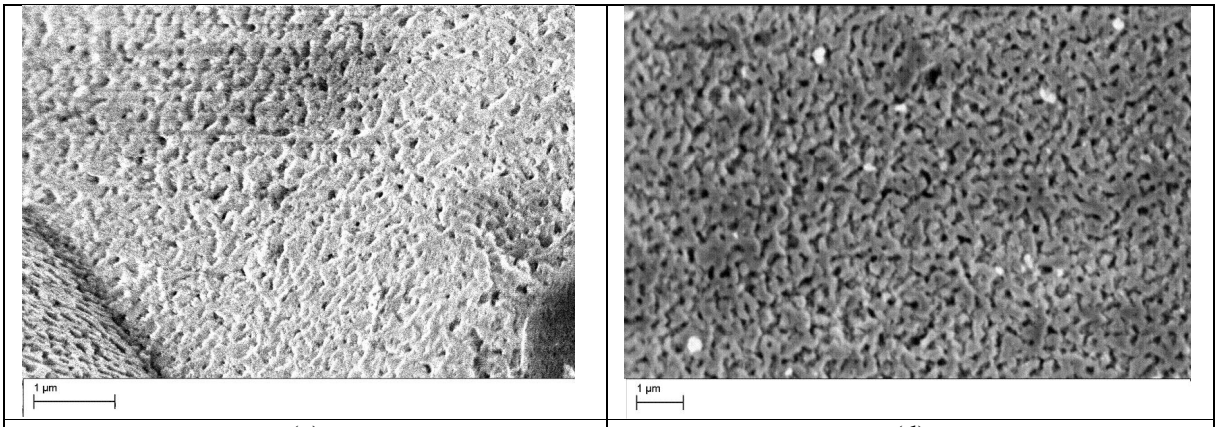

(c) (d)

Figure 11: SEM photograph of phase separated glasses of composition (a) A (650°C x 14 h) and (b) AA (650°C x 14 h). (c) E-II (650°C x 14 h) and (d) EE (650°C x 14 h).

Figure 12 presents the SEM micrograph of leached glasses of composition C (7wt% ZrO_2), heat treated at various temperatures and times. The formation of columnar cristobalite crystals is observed (see Figure 12 b) when the heat-treatment temperature is increased from 650 °C to 700 °C. From FTIR analysis (see Figure 9) of the same sample, heat treated at 700 °C, a small peak around 610–627 cm^{-1} was identified and believed due to crystallisation. Crystallisation was also detected by XRD analysis (see Figure 12 d) when the heat treatment temperature was increased to 700 °C.

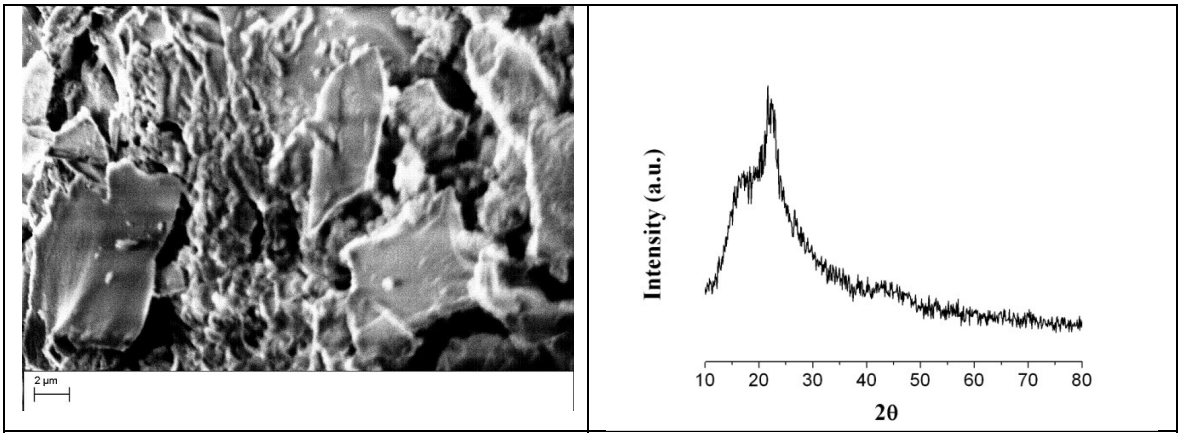

(a) (c)

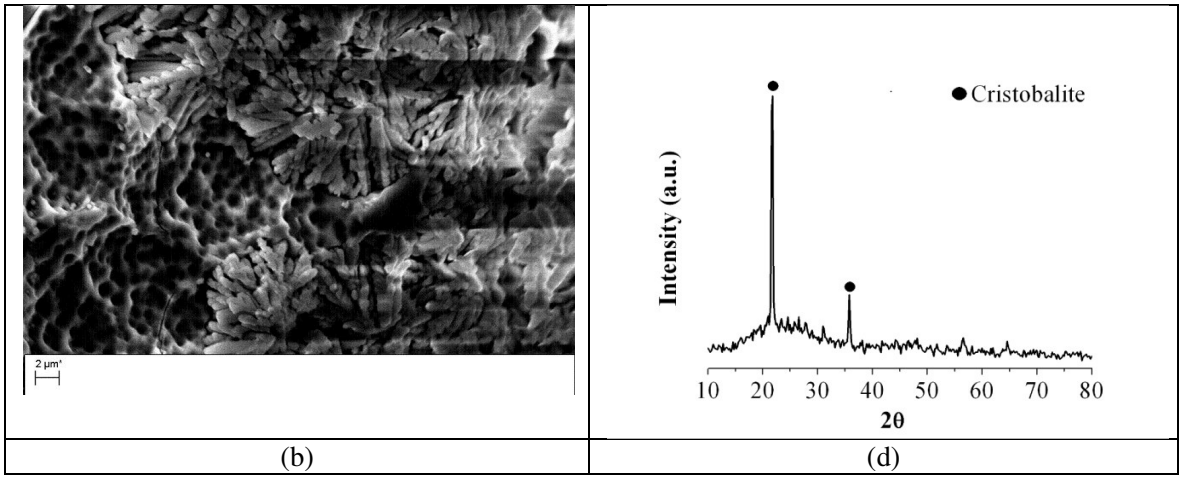

(b) (d)

Figure 12: SEM photographs of leached glass C heat-treated for (a) 650°C x 24 h; (b) 700°C x 14 h; and their XRD patterns (c) 650°C x 24 h; (d) 700°C x 14 h.

The pore characteristics of the glass compositions measured by mercury porosimetry are presented in Table 3. The mean pore size of the porous glass decreased with addition of $ZrO_2/ZrSiO_4$ into the sodium borosilicate system. This effect can be attributed to the larger size of Zr^{+4} ions and their lower mobility which hinders the diffusion processes. Thus the amorphous phase separation process slowed which resulted in smaller pore size. The mean pore size of the porous glass increased with increased duration of the heat-treatment while keeping the temperature constant.

Table 3: Effect of thermal treatment on pore characteristics of different glass compositions

Glass	Thermal treatment		Specific surface area (m^2/g)	Pore volume (cm^3/g)	pore volume <1000 nm %	Mean pore diameter (nm)
	Temperature (°C)	Period (h)				
A	650	24	2.9	0.596	19	240
B	650	24	8.3	0.296	58	58
C	650	24	1.6	0.066	32	61
C	700	14	3.4	0.355	46	186
D	650	24	8.0	0.440	27	85
E	650	24	6.1	0.192	21	41
AA	650	14	12.4	0.553	66	80
AA	650	24	8.6	0.678	44	115
AA	650	63	5.2	0.566	39	139
E-II	650	14	34.9	1.096	44	41
E-II	650	24	18.2	0.678	55	59
E-II	650	63	8.0	0.896	24	139
EE	650	14	31.4	0.407	93	52
EE	650	24	28.7	0.964	69	65
EE	650	63	13.0	1.024	38	115

3.5 Alkali resistance

The alkali resistance of the porous glasses is shown in Table 4. There are many factors which influence the alkali resistance, especially the surface area. The surface area is used in calculating the weight loss in accordance with standard procedure ISO 695 [34]. High surface area and interconnected structures can be achieved where glass composition is properly selected and optimum heat treatments applied. In this study, the glasses with higher surface area and interconnected pore structure were achieved in the glasses series AA–EE and E-II, which had lower amounts of alkali oxide (6 wt% Na_2O). Alkali resistance of the porous glasses was improved by the addition of ZrO_2 or $ZrSiO_4$. The alkali resistance of the porous glass of composition EE is 3–4 times superior to that of porous glass obtained from composition AA without ZrO_2 or $ZrSiO_4$. At the same time, $ZrSiO_4$ containing porous glass (EE) is found to be more alkali resistant than that of ZrO_2 containing glass (E-II) of the same composition. The alkali resistance remains almost constant for the glass series A–E, which has a higher amount of alkali oxide (10 wt% Na_2O). For these glasses the phase separation process is believed to be dominated by nucleation and growth, as opposed to spinodal decomposition.

Table 4: ZrO_2/ $ZrSiO_4$ content and alkali resistance of various porous glasses

Glass	Thermal treatment		ZrO_2 content	$ZrSiO_4$ content	Weight loss
	Temperature (°C)	Period (h)	(wt%)	(wt%)	(mg/dm^2)
A	650	24	0	0	0.3032
B	650	24	3	0	0.3016
C	650	24	7	0	0.6527
D	650	24	11	0	0.3088
E	650	24	15	0	0.3065
AA	650	14	0	0	0.3461
AA	650	24	0	0	0.2830
AA	650	63	0	0	0.2360
E-II	650	14	15	0	0.1872
E-II	650	24	15	0	0.3275
E-II	650	63	15	0	0.2273
EE	650	14	0	15	0.0862
EE	650	24	0	15	0.1812
EE	650	63	0	15	0.2087

4. Summary and Conclusion

DTA and dilatometry can be used to determine basic thermal properties such as glass transition temperature, dilatometric softening temperature and linear thermal expansion coefficient of sodium borosilicate glass. Additions of ZrO_2/$ZrSiO_4$ increases the glass transition temperature. A sharp exothermic peak was observed in the DTA curve for the glass composition containing $ZrSiO_4$. This sharp peak suggests bulk crystallisation. A similar glass composition with ZrO_2 replacing $ZrSiO_4$ showed a broad exothermic effect which is likely associated with surface crystallisation. A TTT diagram was plotted to display the ranges of onset crystallisation temperatures and times and heat treatment temperature and time needed to achieve phase separation, without crystallisation. FTIR analysis was used to investigate the extent of phase separation for glass compositions subject to different heat-treatments. Additions of ZrO_2/$ZrSiO_4$ to the sodium borosilicate glass system reduced the growth rate of phase separation. As a result, mean pore size of the porous glass decreased with addition of ZrO_2/$ZrSiO_4$. For longer heat-treatment times, mean pore size increased. Alkali oxide content in the glass composition was

found to play an important role in the phase separation mechanism. Where 6 wt% of alkali oxide (Na_2O) was used, interconnected pore structures with higher pore volumes were achieved, whereas glasses with 10 wt% of Na_2O yielded spherical droplets with low pore connectivity. Alkali resistance of the porous glasses increased with addition of $ZrO_2/ZrSiO_4$. These glasses were 3-4 times more alkali resistant than the basic sodium borosilicate glass.

5. References:

[1] W. Haller, Application of controlled pore glass in solid phase biochemistry, in: W. H. Scouten (Ed), Solid Phase Biochemistry, John Wiley & Sons, New York, 1983, pp. 535-597.

[2] J. E. Shelby, M. Lopes, Introduction to Glass Science and Technology, second ed., The Royal Society of Chemistry, Cambridge, 2005.

[3] W.-. Du, K. Kuraoka, T. Akai, T. Yazawa, Study of kinetics of the phase separation in sodium borate glasses, J. Mater. Sci. 35 (2000) 3913-3921.

[4] M. J. Plodinec, Borosilicate glasses for nuclear waste imobilisation, Glass Technol. 41 (2000) 186-192.

[5] J. D. Vienna, Nuclear waste vitrification in the united states: Recent developments and future options, Int. J. Appl. Glass Sci. 1 (2010) 309-321.

[6] M. Arab, C. Cailleteau, F. Angeli, F. Devreux, L. Girard, O. Spalla, Aqueous alteration of five-oxide silicate glasses: Experimental approach and monte carlo modeling, J. Non Cryst. Solids 354 (2008) 155-161.

[7] J. Park, S. Lee, Mechanism of preventing crystallisation in low-firing Glass/Ceramic composite substrates, J. Am. Ceram. Soc. 78 (1995) 1128-1130.

[8] R.R. Tummala, Ceramic and glass-ceramic packaging in the 1990s, J. Am. Ceram. Soc. 74 (1991) 895-908.

[9] B.A. Proctor, B. Yale, Glass-fibers for cement reinforcement, Philos. Trans. R. Soc. Lond. Ser. A-Math. Phys. Eng. Sci. 294 (1980) 427-436.

[10] Y. Tsurita, M. Nogami, Preparation of porous supports in the SiO_2-ZrO_2-Na_2O system from microspherical silica gels, J. Mater. Sci. 36 (2001) 4365-4375.

[11] S. Scholes, F.C.F. Wilkinson, Glassy phase separation in sodium borosilicate glasses, Discuss. Faraday Soc. 50 (1970) 175-181.

[12] O.V. Mazurin and E.A. Porai-Koshits, Phase Separation in Glass, Amsterdam, the Netherlands, 1984.

[13] T. Yazawa, H. Tanaka, K. Eguchi, S. Yokoyama, Novel alkali-resistant porous glass prepared from a mother glass based on the SiO_2-B_2O_3-RO-ZrO_2 (R = mg, ca, sr, ba and zn) system, J. Mater. Sci. 29 (1994) 3433-3440.

[14] R.G. Simhan, Chemical durability of ZrO_2 containing glasses, J. Non Cryst. Solids 54 (1983) 335-343.

[15] K. Nakashima, K. Noda, K. Mori, Time-temperature-transformation diagrams for borosilicate glasses and preparation of chemically durable porous glasses, J. Am. Ceram. Soc. 80 (1997) 1101-1110.

[16] J. Kerc, S. Srcic, Thermal analysis of glassy pharmaceuticals, Thermochim. Acta 248 (1995) 81-95.

[17] M. Reben, H. Li., Thermal stability and crystallisation kinetics of MgO-Al_2O_3-B_2O_3-SiO_2 glasses, Int. J. Appl. Glass Sci. 2 (2011) 96-107.

[18] W.D. Kingery, D.R. Uhlmann, H.K. Bowen, Introduction to Ceramics, second ed., John Wiley & Sons, New York, 1976.

[19] N.P. Bansal, R.H. Doremus, Handbook of Glass Properties, Academic Press, Orlando, 1986.

[20] M.M. Lima, R. Monteiro, Characterisation and thermal behaviour of a borosilicate glass, Thermochim. Acta 373 (2001) 69-74.

[21] T. Wakasugi, L.L. Burgner, M.C. Weinberg, A DTA study of crystal nucleation in Na_2O–SiO_2 glasses, J. Non Cryst. Solids 244 (1993) 63-73.

[22] A. Hu, K. Liang, M. Li, D. Mao, Effect of nucleation temperatures and time on crystallisation behaviour and properties of Li_2O–Al_2O_3–SiO_2 glasses, Mater. Chem. Phys. 98 (2006) 430-433.

[23] M.J. Cattell, T.C. Chadwick, J.C. Knowles, R.L. Clarke, D.Y.D. Samarawickrama, The nucleation and crystallisation of fine grained leucite glass-ceramics for dental applications, Dent. Mater. 22 (2006) 925-933.

[24] M.S. Hernández-Crespo, M. Romero, J.M. Rincón, Nucleation and crystal growth of glasses produced by a generic plasma arc-process, J. Eur. Ceram. Soc. 26 (2006) 1679-1685.

[25] A.P. Novaes de Oliveira, A. Bonamartini Corradi, L. Barbieri, C. Leonelli, T. Manfredini, The effect of the addition of $ZrSiO_4$ on the crystallisation of $30Li_2O/70SiO_2$ powdered glass, Thermochim. Acta 286 (1996) 375-386.

[26] W. Vogel, N. J. Kreidl, E. Lense, Chemistry of Glass, American Ceramic Society, Columbus, Ohio, 1985.

[27] A. Agarwal, K.M. Davis, M. Tomozawa, A simple IR spectroscopic method for determining fictive temperature of silica glasses, J. Non Cryst. Solids 185 (1995) 191-198.

[28] Y. Kato, H. Yamazaki, M. Tomozawa, Detection of phase separation by FTIR in a liquid-crystal-display substrate aluminoborosilicate glass, J. Am. Ceram. Soc. 84 (2001) 2111-2116.

[29] S. Fujita, Y. Kato, M. Tomozawa, IR peak shift due to phase separation of Na_2O–SiO_2 system glasses, J. Non Cryst. Solids 328 (2003) 64-70.

[30] P. Pisciella, M. Pelino, FTIR spectroscopy investigation of the crystallisation process in an iron rich glass, J. Eur. Ceram. Soc. 25 (2005) 1855-1861.

[31] M. Lubas, M. Sitarz, Z. Fojud, S. Jurga, Structure of multicomponent SiO_2–Al_2O_3–Fe_2O_3–CaO–MgO glasses for the preparation of fibrous insulating materials, J. Mol. Struct. 744–747 (2005) 615-619.

[32] E.F. Medvedev, Determination of sodium borosilicate bands in the IR spectrum of a multicomponent batch, Glass Ceram. 64 (2007) 300-304.

[33] B.R. Wheaton, A.G. Clare, Evaluation of phase separation in glasses with the use of atomic force microscopy, J. Non Cryst. Solids 353 (2007) 4767-4778.

[34] ISO 695, Glass - Resistance to Attack by Boiling Aqueous Solution of Mixed Alkali - Method of Test and Classification, Third edition, International Organization for Standardization, 1991.